Molecular motors in conservative and dissipative regimes

R. Perez-Carrasco and J. M. Sancho

Departament d'Estructura i Constituents de la Matèria, Universitat de Barcelona, Carrer Martí i Franquès 1, E-08028 Barcelona, Spain

(Received 23 June 2011; revised manuscript received 30 August 2011; published 14 October 2011)

We present a theoretical study of a rotatory molecular motor under a conservative torque regime. We show that conservative and dissipative regimes present a different observable phenomenology. Our approach starts with a preliminary deterministic calculation of the motor cycle, which is complemented with stochastic simulations of a Langevin equation under a flashing ratchet potential. Finally, by using parameter values obtained from independent experimental information, our theoretical predictions are compared with experimental data of the F_1-ATPase motor of the *Bacillus* PS3.

DOI: 10.1103/PhysRevE.84.041915 PACS number(s): 87.16.A−, 05.40.−a, 87.16.Nn, 87.15.Ya

I. INTRODUCTION

Molecular motors are the machinery of the cell whose energetic input is either chemical energy such as the hydrolysis of a nucleotide or the ion flux across a membrane [1–8] following the corresponding physical and chemical laws [1,2]. There is a rich variety of molecular motors: linear ones such as kinesin and myosin [3,4] and rotatory ones such as the bacterial flagellar motor and F_1-ATPase [5–8]. These devices are involved in different tasks such as transport of vesicles along the neural axon, propulsion, pumping, and muscle contraction.

The F_0F_1-ATPsynthase motor is a rotatory reversible machine composed of two main motor parts F_1 and F_0, which are joined through the central γ shaft [9]: F_1 works with the hydrolysis or catalysis of ATP while F_0 works with an ion flux [8,10]. In its direct working regime, F_1F_0-ATPsynthase uses the energy available from an ion gradient to synthesize ATP from its hydrolysis products. Reversibly, for adequate concentrations of ions and nucleotides, F_1 can hydrolyze ATP driving the F_0, which is now acting as an ion pump [5]. Moreover, the F_1 motor part can be isolated by generating a rotatory motion of the γ shaft out of the hydrolysis of ATP. In this regime, the F_1 motor part is called F_1-ATPase.

Initial experiments were done by attaching a micrometric load to the shaft [11,12]. From the tracking of the load, the angular trajectory of the shaft became available, thus making it possible to study the velocity of the motor and its dependence on the ATP concentration and the friction of the load [13–15]. An experimental assay using attached magnetic or dielectric beads [16,17] allowed one to exert a constant torque τ_c on the motor that can either assist or hinder the motion.

All these experiments indicate that the torque applied on molecular motors is an important control parameter to understand the internal dynamic mechanisms of these devices. There are two physical ways to impose an external torque on the motor: One is the above-mentioned conservative torque τ_c acting directly on the motor, while the other is the torque exerted by the drag of the load attached to the motor axis, which produces a dissipative torque. While the former can be controlled directly by the experimental setup, the dissipative torque is an indirect observable depending on the velocity of the motor and the rotational friction coefficient of the attached load. Moreover, the domains of both torques are different. Dissipative torques always operate with positive velocities. In contrast, the domain of conservatives torques is not bounded and works with both positive and negative velocities.

A previous study allowed us to understand quantitatively the working of the motor in the purely dissipative case [18]. The aim of this paper is to extend our approach to accommodate the conservative regime as well. Moreover, using experimental information, we will apply our model to interpret the experimental data for the velocity of the F_1 motor of the *Bacillus* PS3.

The structure of the paper starts with the extension of the model presented in Ref. [18]. We study the effects of the conservative torque in the different processes composing the cycle of the motor. We then describe how to obtain the specific parameter values of the model from the chemical experimental information on F_1. We continue with the explicit development of the deterministic analysis applied to this particular motor and its comparison with the available physical experimental and stochastic simulation results. Finally, we end with a summary and perspectives.

II. MODEL

The average velocity ω of any rotatory motor can be calculated from the ratio between the total length $\theta(t_T)$ advanced versus the corresponding time spent t_T. Since a molecular motor performs its function in closed identical cycles, the mean velocity of the motor can be calculated as the mean velocity along a complete cycle [18–20]. In this cycle, the motor advances a certain characteristic angular distance $\theta_0 = 2\pi/3$, which is fixed by the biomolecular structure of the motor. In contrast, each cycle is composed of a set of processes that last different average times t_i. Therefore, our first guess to estimate the velocity of the motor is

$$\omega = \frac{\theta_0}{\sum t_i}, \tag{1}$$

where the summation runs over all the different processes composing the cycle.

Hence, in order to obtain an expression for ω, the nature of the processes making up one step must be clarified to get an estimation of the corresponding t_i. Since the aim of this analysis is to reproduce the average velocity of the motor, it is not necessary to know the particular time distribution for each t_i, but only its mean value. Therefore, this approach allows us to get a preliminary analytical expression for the torque-velocity

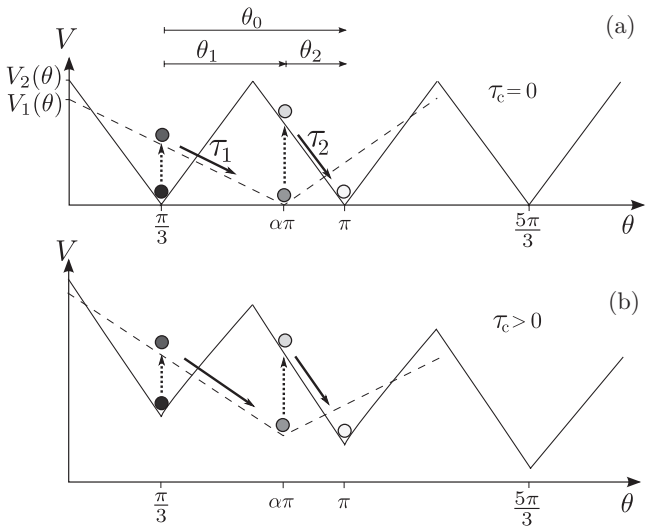

FIG. 1. Scheme of the dynamics of the F_1-ATPase. The shaft (circle) advances by the force introduced from the flashing between the relaxed potential (solid line) and the excited potential (dashed line). Solid thick arrows show the advance of the shaft along each substep under the corresponding torques τ_1 and τ_2, while dashed thick arrows point out the different flashings occurring along the step and correspond to conformational changes of the molecule. The grayscale used for coloring the shaft indicates the time evolution of each step (from darker to lighter tones). The scheme is presented for (a) the pure dissipative case without external torque and (b) an external conservative torque $\tau_c > 0$ assisting the motion of the shaft.

curves without the complicate chemical kinetic pathways of such motors.

Experimental measures point out two well-differentiated alternating behaviors of the shaft: dwell (chemical) and advancing (mechanical) times [13–15]. During the dwell times, the motor fluctuates around a steady-state position. In contrast, during each mechanical time it advances one substep. The whole step is composed of two differentiated substeps of size $\theta_1 = \alpha\theta_0$ and $\theta_2 = (1-\alpha)\theta_0$, where the ratio α is observed experimentally to be $\alpha \simeq 0.7$ [13].

A more detailed analysis of the shaft dynamics can be described by a Langevin equation with a flashing ratchet mechanism between two different sawtooth potentials V_1 and V_2. Each potential represents one conformation state of the protein, namely, an occupied catalytic site V_1 and a free catalytic site V_2 with their corresponding torques τ_1 and τ_2 (Fig. 1).

With the presented elements, the cycle operation can be analyzed. The energetic transduction cycle starts with the motor in its relaxed state V_2 (empty catalytic site) waiting for an ATP molecule (Fig. 1). Once an ATP molecule arrives at this site and the hydrolysis starts, it produces a conformational change of the motor to its excited state ($V_2 \rightarrow V_1$). The excited potential drives the shaft to its minimum advancing the first substep θ_1. Then the shaft jiggles around this minimum. During this catalytic dwell, the hydrolysis products are released to the media. After that, the motor recovers the empty relaxed conformation ($V_1 \rightarrow V_2$) producing the second substep θ_2. Now the cycle is completed and the motor is again in its relaxed conformation with an empty catalytic site, waiting for the next ATP molecule.

A. Mechanical times

Since there are two different substeps, there will be two different mechanical times. Considering an overdamped regime in which the inertial force is neglected over the friction of the system (due to its low Reynolds number), the deterministic dynamics during the mechanical times are described as

$$(\gamma_0 + \gamma_L)\,\omega_i = \tau_i + \tau_c, \tag{2}$$

where γ_0 is the internal friction of the shaft inside F_1, γ_L is the friction of the load with the medium, τ_i is the motive torque that the molecule applies on the shaft, and τ_c is the external conservative torque applied to the load. The subindex i can take two values $i = \{1,2\}$ for each substep. The subindex 1 corresponds to the first substep caused by the excited potential and subindex 2 corresponds to the second substep caused by the relaxed one.

In Eq. (2), ω_i is the velocity along the mechanical time t_{mech_i}. Both terms are related through the specific substep distance $\Delta\theta_i$,

$$t_{\mathrm{mech}_i} = \frac{\Delta\theta_i}{\omega_i} = \Delta\theta_i \frac{\gamma_0 + \gamma_L}{\tau_i + \tau_c}. \tag{3}$$

The effective torque acting on the shaft $\tau_i + \tau_c$ produces a tilting of the driving potential (Fig. 1). Additionally, in contrast to the purely dissipative case, if a conservative torque is present, there is a constant torque acting on the load even during the dwell times. Therefore, when the shaft is in a potential minimum, its spatial distribution is shifted and the expected spatial position of the particle does not coincide with the minimum of the potential (Fig. 2). Hence this changes the effective distance to cover for the next mechanical step once the excitation occurs. An assisting torque will reduce the distance to cover while a hindering torque increases it. The new average starting position for the step can be analytically estimated from the equilibrium distribution $P(\theta)$ around the minimum of the relaxed potential, which can be approximated as an infinite linear piecewise well [21]. Accordingly, the probability is divided in two parts: P_- for $\theta < 0$ and P_+ for $\theta > 0$ [22], which for the ATP dwell are

$$P_-(\theta) \simeq \frac{1}{k_B T}\left(\frac{1}{\tau_c+\tau_2} - \frac{1}{\tau_c-\tau_2}\right)^{-1} e^{(\tau_c+\tau_2)\theta/k_B T}, \tag{4}$$

$$P_+(\theta) \simeq \frac{1}{k_B T}\left(\frac{1}{\tau_c+\tau_2} - \frac{1}{\tau_c-\tau_2}\right)^{-1} e^{(\tau_c-\tau_2)\theta/k_B T}. \tag{5}$$

The value of the shift $\delta\theta(\tau_c)$ is

$$\delta\theta(\tau_c) = \langle\theta\rangle = \int_{-\infty}^{\infty} \theta\, P(\theta) d\theta = k_B T \frac{2\tau_c}{\tau_2^2 - \tau_c^2}, \tag{6}$$

which is a purely thermal phenomenon. Without thermal fluctuations, the average relaxed position would coincide with the minimum of the relaxed potential.

Equation (6) will be valid only if the dwell time is long enough to allow the shaft to reach the equilibrium probability

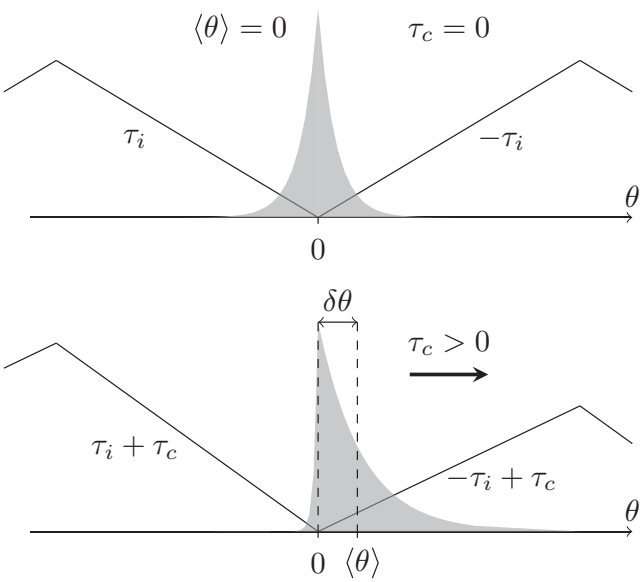

FIG. 2. Effect of a conservative torque in the equilibrium probability distribution of the shaft (gray shade) in the minimum of a piecewise well (solid line). When no external torque is considered (top case) the profile is symmetric and centered in the minimum of the potential, while an external applied force (bottom case) shifts the profile so the average position of the shaft does not coincide with the minimum of the potential.

distribution. In the case of the second substep, the catalytic dwell time prior to the second stroke is not long enough to reach the equilibrium distribution [13]. Hence the shift advance for $\Delta\theta_2$ will not be taken into account.

With Eq. (6) and the definition in Eq. (3), we get the two mechanical times using $\Delta\theta_1(\tau_c) = \theta_1 - \delta\theta(\tau_c)$ and $\Delta\theta_2 = \theta_2$ with the corresponding torques τ_1 and τ_2. Therefore, the contribution of an external conservative torque not only is that of modifying the total torque through Eq. (2) but also alters the distances to cover in a mechanical substep.

B. Chemical times

Chemical times are the lapses when there is no shaft advance. Due to the enzymatic nature of such times, the dwell chemical time depends on the inverse of the ATP concentration t_{ATP}. The remaining catalytic times are grouped into t_0 and stand for the rest of the reactions independent of [ATP], such as the release of products to the media or other internal tasks needed by the motor [16,23]. These two contributions can be grouped as

$$t_{\mathrm{chem}} = t_{\mathrm{ATP}} + t_0 = \frac{1}{k_{\mathrm{ATP}}[\mathrm{ATP}]} + t_0 \equiv t_0\left(\frac{k_M}{[\mathrm{ATP}]} + 1\right), \tag{7}$$

which has been rewritten in terms of a Michaelis-Menten relation, in agreement with the average dwell time observed in experimental data [13,18]. This expression also gives the relation between the catalytic constant k_{ATP} and the effective Michaelis-Menten constant k_M,

$$k_M = (k_{\mathrm{ATP}} t_0)^{-1}. \tag{8}$$

However, even though during the chemical times there is no mechanical stroke acting on the shaft, their duration may be affected by the external forces. It has been observed experimentally that an assisting conservative torque reduces the dwell times while a hindering torque increases them [17]. Similar results have been observed for other molecular motors [3]. An accepted theory to explain this phenomenon is that the catalytic site is deformed due to the external force [24]. The steric effects of this deformation change the probability of the ATP molecule reaching its catalytic site. This phenomenon is equivalent to considering the external torque as an external catalyst or inhibitor in the reaction [25].

We assume now that k_{ATP} can be approximated by a linear function of the external torque,

$$k_{\mathrm{ATP}} = k_0 + k_1\,\tau_c, \tag{9}$$

where the parameters k_0 and k_1 can be obtained from the experimental data, as will be explained in Sec. III.

With the description of the different dwell and mechanical processes, the total time for a cycle becomes available and the angular velocity can be computed. This is done by introducing Eqs. (3), (7), and (8) into Eq. (1),

$$\langle\omega\rangle([\mathrm{ATP}],\tau_c) = \frac{\theta_0}{[\theta_1 - \delta\theta(\tau_c)]\frac{\gamma_0+\gamma_L}{\tau_c+\tau_1} + \theta_2\frac{\gamma_0+\gamma_L}{\tau_c+\tau_2} + t_0\left(1 + \frac{k_M(\tau_c)}{[\mathrm{ATP}]}\right)}. \tag{10}$$

This is a simple analytical expression that will give information on the chemical and mechanical substeps' relevance.

C. Stochastic simulations

The energetic processes involved in the motion of the motor are larger but comparable to the thermal energy and a correct theoretical study should include thermal fluctuations [26,27]. In fact, thermal fluctuations are partially included in the shift $\delta\theta$ [Eq. (6)], which is a thermal effect. Actually, thermal effects can be extensively studied along the whole trajectory from the simulation of the overdamped Langevin equation describing the dynamics of the system. This is achieved by adding the thermal force on Eq. (2),

$$(\gamma_0 + \gamma_L)\dot{\theta} = -V'(\theta,t) + \tau_c + \xi(t), \tag{11}$$

where $\xi(t)$ is a Gaussian white noise of correlation

$$\langle\xi(t)\xi(t')\rangle = 2k_B T(\gamma_0 + \gamma_L)\delta(t - t') \tag{12}$$

and $-V'(\theta,t)$ is the corresponding torque of the flashing potential,

$$V(\theta,t) = V_1(\theta) + [V_2(\theta) - V_1(\theta)]\eta(t). \tag{13}$$

The flashing mechanism of the potential is determined by the time-dependent function $\eta(t)$, which can switch between two values 0 and 1. If the motor is in the excited one, $\eta = 0$, which results in $V(\theta,t) = V_1(\theta)$; if the motor is in the relaxed one, $\eta = 1$, which results in $V(\theta,t) = V_2(\theta)$.

In order to carry out the simulations, we propose explicit transition times between both states, which depend on the working of the motor and must be extracted from the experimental observation of trajectories. The most important source of stochasticity is observed experimentally to be that

of the ATP dwell time s, which is observed to follow a two-step rate-limiting reaction that can be well approximated by a single-step first-order reaction with an exponential distribution [28]

$$P(s) = \frac{e^{-sk_{\mathrm{ATP}}[\mathrm{ATP}]}}{k_{\mathrm{ATP}}[\mathrm{ATP}]}, \tag{14}$$

which has a mean dwell time of $(k_{\mathrm{ATP}}[\mathrm{ATP}])^{-1}$, as seen in Eq. (7).

In contrast, the catalytic release time t_0 and the mechanical times have not been seen to have a relevant variation in time. Several simulations considering stochasticity in t_0 and t_{mech} have been carried out without obtaining variations in the resulting velocity. Therefore, they will be considered constant from here on.

Once the times are well defined, the flashing potential can be simulated with the occupation times $t_{\mathrm{excited}} = t_{\mathrm{mech1}} + t_0$, which is constant in time, and $t_{\mathrm{relaxed}} = t_{\mathrm{mech2}} + s$, where s is random following Eq. (14). The numerical simulations are performed using standard algorithms. More information can be found in Ref. [18].

III. MODEL PARAMETERS OF F_1-ATPASE FOR *BACILLUS* PS3

Up to now, all the parameters of the model have been identified for a generic F_1-ATPase rotatory motor. In this section we show how to obtain their effective values for the specific F_1 motor of *Bacillus* PS3.

There is a great variety of F_1-ATPase rotatory motors, each one operating in different scenarios. Our model can incorporate these differences in the model parameters, which have to be evaluated for each particular case and set of circumstances. In doing so we have to use the available experimental information concerning chemical reaction rates, experimental torques, etc., avoiding the use, if possible, of a fit of the experimental velocities. The model parameters for *Bacillus* PS3 have been obtained as follows.

First of all, it is useful to split the parameters into three groups. One group includes those parameters that are controlled externally through the experiment. They are usually the concentration of [ATP], the external conservative torque τ_c, and the friction of the load attached to the gamma shaft γ_L.

A second group comprise those parameters that are specific to the *Bacillus* PS3 F_1 motor. They do not change with the external conditions. These block include the internal motive torques of the motor τ_1 and τ_2, the free energy used in a step ΔG_{ATP}, and the internal friction of the shaft γ_0. Since these parameters are independent of the realization, their values can be extracted from different experimental setups. Actually, the torque τ_1 can be obtained from recent experiments performed with the ADP-inhibited form of F_1 [16]. These experiments unravel the sawtooth potential form of the excited potential around its minimum (corresponding to the first substep) and a value of $\tau_1 = 35 \pm 2$ pN nm can be extracted (Fig. 3). This value is in agreement with an alternative experiment in which the stalling force of the motor was seen to be approximately -40 pN nm [17]. Accordingly, the value of the torque applied

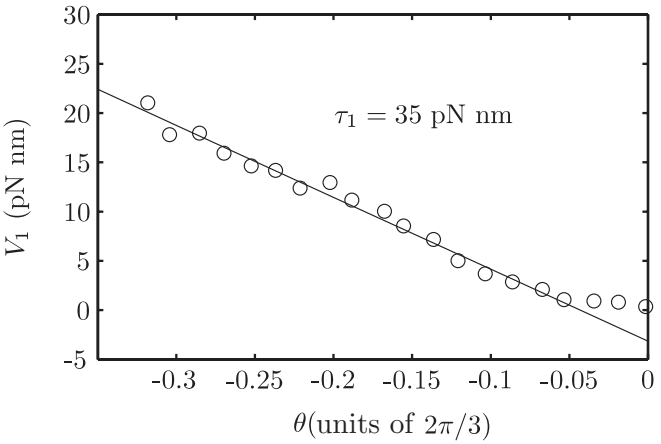

FIG. 3. Experimental values for the excited potential (circles) to the left of its minimum. The potential introduces a torque of $\tau_1 = 35 \pm 2$ pN nm. Data are extracted from Ref. [16].

from the relaxed potential for the second substep τ_2 can be obtained from ΔG_{ATP} and τ_1 using the energy balance relation

$$\Delta G_{\mathrm{ATP}} = \tau_1\theta_1 + \tau_2\theta_2, \tag{15}$$

which returns a value $\tau_2 \simeq 58$ pN nm. From this last analysis we have to expect a larger torque in the second substep. Moreover, as different F_1 motors operate in similar work regimes, with the same free energy ΔG it is expected that these values are shared with other F_1 motors [14].

A third group consists of the parameters that are sensitive to the particular experimental conditions. These parameters are, in general, those related to the chemical kinetics of the motor, which are k_1, k_0, and t_0. The parameters k_1 and k_0 can be obtained from experimental data of k_{ATP} in Ref. [17]. The linear fit is shown in Fig. 4 and the explicit values obtained are in Table I. The catalytic dwell parameter $t_0 \sim 0.6$ ms is guessed by taking a reaction rate ratio that is equivalent to that in Ref. [13]. These values for the reaction rate at zero conservative torque (in the dissipative regime) return a value that is different from previous experiments [13]. This is a clear signature of the difference in concentration of ATP, ADP,

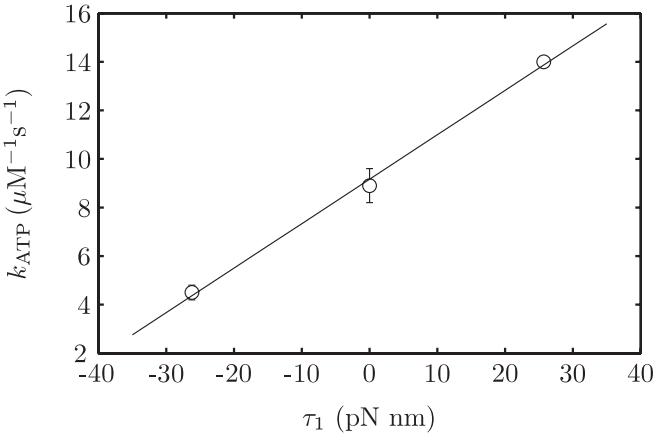

FIG. 4. Experimental results for the ATP binding constant. The linear approximation in Eq. (9) for the binding fits well with the experimental values extracted from Ref. [17].

TABLE I. Table of parameters used in the theoretical calculations and numerical simulations for the $PS3\,F_1$.

	Parameter	Value
Control Parameters	[ATP]	
	τ_c	
	γ_L	0.14 pN nm s
Motor Intrinsic Parameters	ΔG	90 pN nm
	τ_1	35 pN nm
	γ_0	0.005 pN nm s
Experimental Setup Parameters	k_1	0.183 $\text{pN}^{-1}\text{nm}^{-1}\,\mu\text{M}^{-1}\,\text{s}^{-1}$
	k_0	9.164 $\mu\text{M}^{-1}\,\text{s}^{-1}$
	t_0	0.6 ms

phosphate, and perhaps other ions changing the ionic strength from both experiments. Hence, all the parameter values are known (Table I) and can be used to compare and predict results of F_1 from *Bacillus* PS3.

IV. RESULTS

A. Average velocity

Preliminary results on the motor velocity are obtained by introducing the parameter values in Eq. (10) for the conservative torque in the wide domain $(-40,60)$ pN nm. The goodness of fit of this prediction can be established by comparing Eq. (10) with experimental curves from Ref. [17]. A good qualitative and partially quantitative match between theory and experiments is found without any free parameter (Fig. 5), thus confirming that the effects of the external conservative torque are well controlled by the model. However, the uncertainty of the experimental error bars may be relevant and more precise experiments could shed further light on the goodness of fit of the theoretical results. Thus, using the same approach as in Ref. [18] for a dissipative regime with the appropriate physical and chemical changes, it is possible to predict the dependence of the mean velocity versus a conservative torque, a friction γ_L [18], and [ATP].

The simulation results are quantitatively similar to those of the deterministic theoretical prediction as seen in Fig. 5. However, simulations show that, in general, the velocity of the motor is slower than the deterministic prediction, as it should be. This effect comes from failed ATP hydrolysis processes that do not produce a successful step, which is magnified for hindering torques, similar to the behavior observed in Ref. [29]. This phenomenon was analyzed theoretically in Ref. [18]. However, the fidelity between simulation and theory shows a certain degree of robustness against thermal fluctuations.

It is interesting to note that the motor does not respond in an equivalent way to the same torque values in different regimes, namely, dissipative or conservative. This can be seen in Fig. 6, where the torque-velocity relation is plotted in both situations.

One particular case of these differences is observed for the stall force of the motor. For a conservative hindering torque, the motor stalls when the torque applied counters the motive torque, $\tau_c(\text{stall}) = -\tau_1$. In contrast, one could guess that a dissipative torque will never be able to stop the motor. Nevertheless, for large enough values of the friction of the load γ_L, the motor velocity decreases so dramatically that the dissipative torque tends to a constant value, which can be

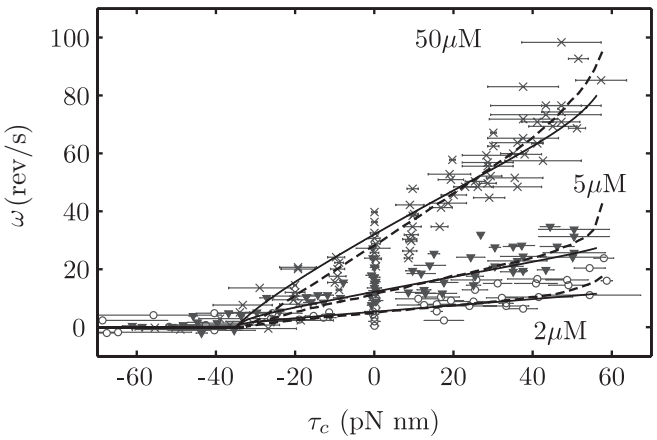

FIG. 5. Angular mean velocity versus conservative torques for three ATP concentrations. Solid lines are the theoretical prediction in Eq. (10), dashed lines correspond to numerical simulations, and symbols are from experimental data [17]. The parameters used are those of Table I.

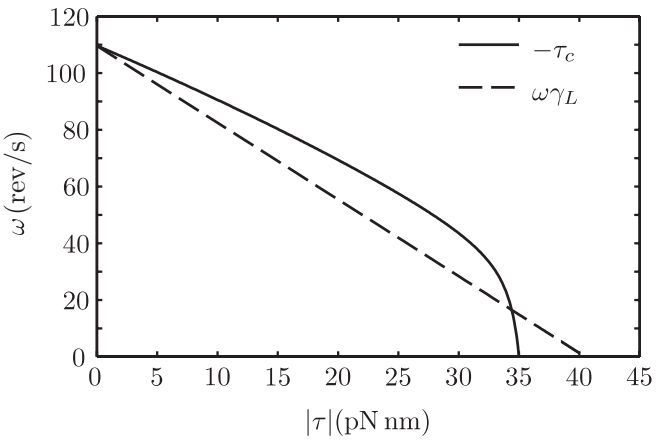

FIG. 6. Comparison between the velocities obtained from Eq. (10) for hindering conservative torques (solid line) and dissipative torques in the same range of values (dashed line). The dissipative torque is obtained through the variation of γ_L. The parameters used are those of Table I and [ATP] = 50 μM.

calculated from Eq. (10),

$$\tau_d(\text{stall}) = \gamma_L \omega|_{\gamma_L \to \infty} = \frac{\theta_0}{\frac{\Delta\theta_1}{\tau_1} + \frac{\Delta\theta_2}{\tau_2}} \simeq 40.5 \text{ pN nm}. \quad (16)$$

This result also shows that the stall dissipative torque can be larger than the internal torques of the motor, which is not the case for the stall conservative torque. This prediction of the model can be checked experimentally.

B. Torque regimes and backstepping

The time distribution proposed in the preceding section for the mechanical times is based on the shift of the equilibrium distribution. It is valid when the external conservative torques are smaller than the internal motive torques of the motor. Once the internal torques are exceeded the motor is not able to retain the shaft and the stepping is not driven by flashing assisting torques but by jumps over a set of potential barriers.

Thus the limiting values of the conservative torques are those of the excited potential, which are lower than the relaxed ones. For values of external torques greater than the motive ones, the experimental information is very poor and no conclusions can be obtained. However, several comments can be made, especially for large hindering torques. Now the motor has two different behaviors: The motor either stalls and stays fixed for large values of the torque or breaks and rotates backward [17]. The stalling regime suggests that the excited state is not stable when the motor goes backward flashing to the relaxed state, which is able to retain the motor. Therefore, in general, the motor is able to retain the shaft for hindering torques larger than the excited advancing torque (Fig. 7).

In contrast, the slippage effect shows that the stalling mechanism does not always work. In terms of our model this would mean that the motor is not able to flash to the relaxed state. It remains in the excited state and hence a high enough hindering torque may cause backward steps. Therefore, this

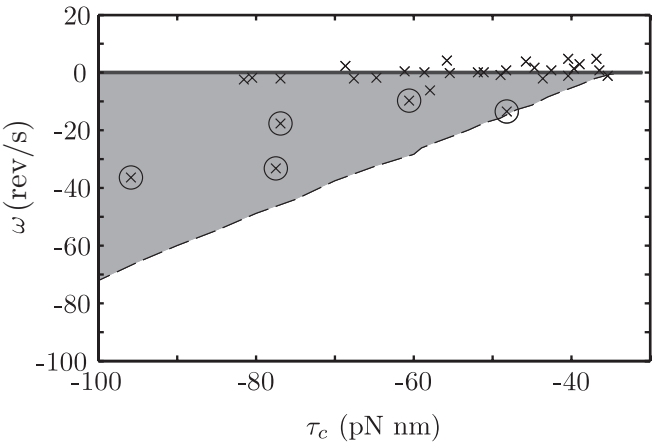

FIG. 7. Different behaviors for high values of hindering torques compared with experimental results (crosses). Usually the motor stays still around $\omega = 0$; however, slippage events (crosses inside circles) allow backward motion. The velocity during the slippage is the one fixed by the excited potential (dashed line), while the measured velocity must be the result of a mixture of both behaviors, fixed and slippage (shaded area). Experimental data are extracted from Ref. [17].

is equivalent to the case of a particle falling along a tilted sawtooth potential. Experiments show that the slippage effect is not permanent, but lasts only a few steps. Therefore, there will be a maximum backward velocity fixed by the velocity of a particle trapped in the excited state. In real experiments, since motors present both behaviors, slippage and rest behavior, the velocity measured must be an intermediate velocity between $\omega = 0$ and the velocity for a fixed excited potential (Fig. 7). Therefore, the phenomenology observed experimentally is explained easily from the framework of our model, which also predicts correctly the velocities observed in each regime.

V. CONCLUSION AND PERSPECTIVES

In this paper the dependence of the velocity of the F_1-ATPase with an external conservative torque has been studied. In contrast to the purely dissipative case, the conservative torque is always present in the dynamics. This scenario has introduced three theoretical elements in the description of the motor dynamics: the effective torque $\tau_i + \tau_c$, the shift of the rest state $\delta\theta$, and the kinetic constant dependence $k_{\text{ATP}}(\tau_c)$. Thus the mechanisms of the stepping altered by the external torque have been identified and quantified. In addition, the values of all the parameters of the model have been extracted from complementary experimental information that is different from the data of Fig. 5. This gives an added value to the predictive power of the model.

Both of our theoretical approaches, deterministic and stochastic, allow us to compare the conservative regime with the dissipative one. Each regime returns a different behavior with a characteristic torque-velocity profile, i.e., for the same value of the torque in each regime, distinct average velocities are obtained. This also implies a different available range of torques and different stall torques. The physical origin of these facts appear because the conservative torque is constant in time while the dissipative torque depends on the instantaneous velocity of the motor.

In order to measure experimentally these predictions, experimental assays are necessary in which the same motor works in the two regimes. These observations must be done in the same experimental conditions since there is a strong dependence on the effective experimental parameters k_1, k_0, and t_0. The measures of these different behaviors in the same setup can give very useful information on the working of the specific motor.

Although the theoretical results are in agreement with the experimental data, there is still much experimental work that remains unclear. Mainly, the uncertainty in the applied torque for each bead is very high, so it is not possible to extract precise values such as the saturation values for the hindering torques. More experimentally accurate quantities could help one obtain more precise values for the torques, which would be useful in predicting a more accurate description of the potentials. This model may be able to determine the extent to which the precision in such parameters must be improved in order to obtain further information on this motor.

Moreover, even though the model returns reliable information on the operation of the motor, the results are limited to a regime in which the external torque does not surpass the values of the internal torques of the potential. Beyond this

parameter region, the model can have different interpretations. A deeper exploration of trajectories under larger torques could unravel interesting properties of the motor. It should be noted that in those regimes, the analytical expression in Eq. (1) needs to be revised since the regular stepping phenomenon is lost.

ACKNOWLEDGMENTS

We acknowledge financial support from Ministerio de Educación y Ciencia of Spain through Project No. FIS2009-13360-C03-01 and Generalitat de Catalunya through Project No. 2009SGR14. R.P.-C. acknowledges Ministerio de Ciencia e Innovación of Spain Grant No. FPU-AP2007-00987.

[1] J. Howard, *Mechanics of Motor Proteins & the Cytoskeleton* (Sinauer, Sunderland, MA, 2001).
[2] M. Schliwa, *Molecular Motors* (Wiley-VCH, Weinheim, 2003).
[3] K. Visscher, M. J. Schnitzer, and S. M. Block, Nature (London) **400**, 184 (1999).
[4] A. B. Kolomeisky and M. E. Fisher, Annu. Rev. Phys. Chem. **58**, 675 (2007).
[5] C. von Ballmoos, A. Wiedenmann, and P. Dimroth, Annu. Rev. Biochem. **78**, 649 (2009).
[6] H. C. Berg, Annu. Rev. Biochem. **72**, 19 (2003).
[7] G. Oster and H. Wang, Trends Cell Biol. **13**, 114 (2003).
[8] M. Yoshida, E. Muneyuki, and T. Hisabori, Nature Rev. Mol. Cell Biol. **2**, 669 (2001).
[9] J. P. Abrahams, A. G. W. Leslie, R. Lutter, and J. E. Walker, Nature (London) **370**, 621 (1994).
[10] P. D. Boyer, Biochim. Biophys. Acta **1140**, 215 (1993).
[11] H. Noji, R. Yasuda, M. Yoshida, and K. Kinosita, Nature (London) **386**, 299 (1997).
[12] R. Yasuda, H. Noji, K. Kinosita, and M. Yoshida, Cell **93**, 1117 (1998).
[13] R. Yasuda, H. Noji, M. Yoshida, K. Kinosita, and H. Itoh, Nature (London) **410**, 898 (2001).
[14] D. Spetzler, J. York, D. Daniel, R. Fromme, D. Lowry, and W. Frasch, Biochemistry **45**, 3117 (2006).
[15] K. Adachi, K. Oiwa, T. Nishizaka, S. Furuike, H. Noji, H. Itoh, M. Yoshida, and K. Kinosita Jr., Cell **130**, 309 (2007).
[16] Y. Hirono-Hara, K. Ishizuka, K. Kinosita, M. Yoshida, and H. Noji, Proc. Natl. Acad. Sci. USA **102**, 4288 (2005).
[17] T. Watanabe-Nakayama, S. Toyabe, S. Kudo, S. Sugiyama, M. Yoshida, and E. Muneyuki, Biochem. Biophys. Res. Commun. **366**, 951 (2008).
[18] R. Perez-Carrasco and J. M. Sancho, Biophys. J. **98**, 2591 (2010).
[19] A. Ciudad and J. M. Sancho, J. Chem. Phys **128**, 225107 (2008).
[20] G. Meacci and Y. Tu, Proc. Natl. Acad. Sci. USA **106**, 3746 (2009).
[21] This is equivalent to considering that the well length is larger than the width of the distribution $P(\theta)$.
[22] See Supplemental Material at http://link.aps.org/supplemental/10.1103/PhysRevE.84.041915 for a full derivation of the equilibrium spatial probability profile of a thermalized particle in an infinite triangular well.
[23] D. Okuno, R. Fujisawa, R. Iino, Y. Hirono-Hara, H. Imamura, and H. Noji, Proc. Natl. Acad. Sci. **105**, 20722 (2008).
[24] N. Naber, T. J. Minehardt, S. Rice, X. Chen, J. Grammer, M. Matuska, R. D. Vale, P. A. Kollman, R. Car, R. G. Yount, R. Cooke, and E. Pate, Science **300**, 798 (2003).
[25] A. Ciudad and J. M. Sancho, Biochem. J. **390**, 345 (2005).
[26] S. Toyabe, T. Okamoto, T. Watanabe-Nakayama, H. Taketani, S. Kudo, and E. Muneyuki, Phys. Rev. Lett. **104**, 198103 (2010).
[27] K. Hayashi, H. Ueno, R. Iino, and H. Noji, Phys. Rev. Lett. **104**, 218103 (2010).
[28] K. Shimabukuro, R. Yasuda, E. Muneyuki, K. Y. Hara, K. Kinosita, and M. Yoshida, Proc. Nat. Acad. Sci. USA **100**, 14731 (2003).
[29] A. Palanisami and T. Okamoto, Nano Lett. **10**, 4146 (2010).